Constrained Order in Nanoporous Alumina with High Aspect Ratio: Smart Combination of Interference Lithography and Hard Anodization

Josep M. Montero Moreno, Martin Waleczek, Stephan Martens, Robert Zierold, Detlef Görlitz, Victor Vega Martínez, Victor M. Prida, and Kornelius Nielsch*

With only two matched processing steps, the fabrication of thick nanoporous alumina membranes with mono-oriented, perfect hexagonal packing of pores, and precise control of all structural parameters over large areas is demonstrated. The cylindrical pores are uniform in shape and widely tunable in their dimensions and spatial distribution, with aspect ratios as high as 500. In brief, electropolished aluminum is first patterned using three-beam interference lithography in a single step and then anodized in a hard regime. The periodic concavities in the aluminum surface guide the pore nucleation, and the self-ordering phenomenon guarantees the maintenance of the predefined arrangement throughout the entire layer. In contrast to other methods, the interpore distance can be easily adjusted, the porous layer is not limited in thickness, no prefabricated stamps are involved, and the periodic pattern can be easily reproduced without risk of degradation. The approach overcomes the time, cost, and scale limitations of other existing processes. These membranes are well-suited for the templated fabrication of perfectly ordered arrays of highly uniform 1D nanostructures. Thus, the application fields of these functional membranes are diverse: magneto-optical and opto-electronic devices, photonic crystals, solar cells, fuel cells, and chemical and biochemical sensing systems, to name a few.

1. Introduction

Nanoporous materials have been used as templates for the fabrication of nanostructure ensembles functioning as basis for the engineering of functional devices as well as fundamental research. Reported studies cover a wide variety of fields such as: electronics and opto-electronics, energy storage, fuel cells, solar cells, thermoelectric generators, catalysis, drug delivery, or chemical and biological sensing.[1–7] The standard nanoporous materials typically exhibit a low degree of order and lack of geometric uniformity. This is a constraint for the high efficiency of nanostructured devices based on them or for the exhaustive research of the nanostructures. The ability to control the complete geometry and spatial distribution of the nanostructures with high accuracy and retain the order over several orders of magnitude becomes crucial in many areas. For instance, the capacity to tune the band structure of a photonic crystal through its geometry leads to significant increasing of lasing action efficiency.[8] The far-field interaction in plasmonic periodic nanostructures highlights the importance of the long-range order to achieve resonance.[9] Techniques such as surface-enhanced Raman spectroscopy, demand highly ordered and precisely controlled nanostructured substrates.[10] Nanostructured solar cells under this long-range order condition stand for promising efficiencies.[11] The understanding of the complex dipolar interactions in arrays of magnetic nanostructures requires high uniformity and precise arrangement to allow for the proper comparison of experimental data and theoretical simulations.[12,13]

Among the different templates used for the fabrication of nanostructures, porous anodic aluminum oxide membranes (AAO) are the most renowned due to their singular characteristics.[14–22] They are an array of densely-packed cylindrical nanopores extending up to several micrometers in length with widely tunable geometry. The fabrication of highly ordered AAO involves the two-step electrochemical oxidation of aluminum under specific conditions that guarantee self-organization of pores.[23] The resulting self-ordered AAO membranes show multiple domains of hexagonally close-packed, randomly-oriented arrays of pores. Each single domain does not extend over more than a few square micrometers. Up to now, one powerful approach has been documented to realize longer stretches. The imprint of a periodic arrangement of nanoconcavities at the aluminum surface defines the pore nucleation sites in a process known as guided anodization.[19] Different methods have been used to generate the nanoconcavities, that is, focused ion beam milling, e-beam lithography, cold or hot nanoimprint lithography, step or flash nanoimprint lithography, dip-pen lithography or colloidal lithography.[24–30] How-

Dr. J. M. Montero Moreno, M. Waleczek, S. Martens, R. Zierold, Dr. D. Görlitz, Prof. K. Nielsch
Institute of Applied Physics
Universität Hamburg
Jungiusstr. 11, 20355, Hamburg, Germany
E-mail: jmontero@physnet.uni-hamburg.de
Dr. V. Vega Martínez, Dr. V. M. Prida
Department of Physics
University of Oviedo
Calvo Sotelo s/n, 33007, Oviedo, Spain

DOI: 10.1002/adfm.201303268

ever, these techniques are restricted to small processing areas, long processing times, lacked tunability of the geometrical parameters, use costly and delicate equipment or need lithographically prefabricated stamps, which are non-recyclable and expensive. Laser interference lithography (LIL) has been proposed as an alternative to overcome these limitations.[31] The technique utilizes the phenomenon of light interference to create 2D periodic patterns in a photoactive polymer film coating a planar surface. LIL is characterized by fast processing times, effortless scalability to wafer size, flexibility on the periodic patterns, easy and wide tunability of the pattern geometry, simple optical setup, low temperature processing, and high repeatability and reproducibility of the process. Its application to industrial scale is also possible.[32] However, when a pattern was desired in a metallic surface by LIL, typically hard or soft patterned stamps had to be first fabricated by LIL and next the pattern had to be transferred into the metallic surface by wet or dry etching or nanoimprinting, approaches known as soft or hard interference lithography.[33–35] The direct application of LIL on aluminum (or any metallic surface) was restricted to extremely flat surfaces and the patterning process could only be demonstrated on sputtered thin films deposited on silicon wafers, which limited the maximum thickness (<1 μm) of the porous membrane.[31] Only ultrathin AAO membranes with small pore aspect ratios (below 20) were feasible and the large versatility of these templates was lost.

There are two standard self-ordered regimens for the fabrication of AAO membranes: Mild and hard anodization. They are only differentiated by the growth mechanism of the porous layer. In mild anodization, migration of ions through the aluminum oxide barrier layer at the bottom of the pores in an electric field controls the growth kinetics.[17] In the hard anodization, the fast migration of ions through the barrier layer requires a high conduction in the pores. This can not be fulfilled by the electrolyte in the pores, limiting the growth kinetics.[19] The resulting membranes differ strongly in their properties. The enhanced mechanical and chemical stabilities of the hard anodized membranes are especially remarkable. The characteristics of the hard anodization prevail over the mild anodization and make this process more attractive with much faster processing times for thick membrane fabrication, broader window of conditions with pore self-organization and comparatively narrower pores, which increases the pore aspect ratio.

In this work, LIL is used to texture the surface of aluminum sheets with a hexagonal array of nanoconcavities. Our LIL setup is based on three-beam interference using a modified Lloyd's Interferometer.[36] It created, after a single exposure, a perfect hexagonal periodic pattern, which is equivalent to the natural pore arrangement in the AAO. The periodicity, or lattice constant, of the interference pattern can be easily adjusted to a wide range of values from 190 to 800 nm. The optimization of the resist layer stack is critical for a successful patterning.[37] After the photoresist development, the organic film, which covers the sample, is patterned with holes and serves as a mask for the subsequent pattern transfer onto the aluminum. The cavities generated on the surface act as pore nucleation sites during the first stages of anodization. The perfectly-ordered AAO are fabricated in hard or mild conditions as long as the periodicity of the LIL pattern matches the interpore distance of the outcoming AAO and the anodization is carried out under pore self-organization. We have focused this work on the outstanding hard anodization and consigning our results regarding the mild anodization to the supporting information. The self-ordering regime assures that after the pore nucleation, the initial arrangement of pores is fully kept during the growth of the porous oxide. By anodizing bulk aluminum, the length of the pores extends up to several micrometers. The aspect ratio of the pores can be as high as 500, which is a prerequisite for the template-assisted fabrication of nanowires, nanotubes and pseudo-1D nanostructures.

2. Results and Discussion

Figure 1 illustrates the fabrication process using bulk aluminum chips and includes photographs of samples at different

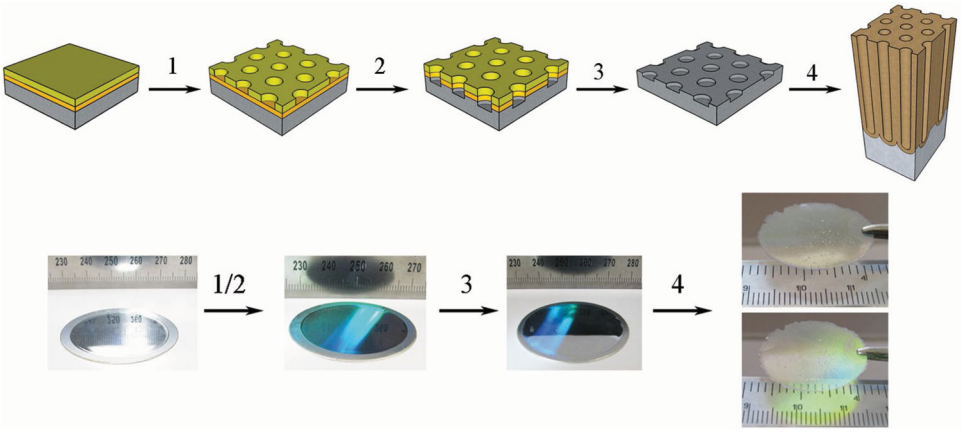

Figure 1. Scheme and pictures showing the fabrication of perfectly-ordered membranes via combination of LIL and aluminum anodization: generation of the periodic pattern by LIL on the photoresist — 1) antireflection coating bilayer spin coated on top of electropolished aluminum; 2) pattern transfer to the aluminum surface by a two-step dry and wet etching process; 3) complete removal of the resist bilayer by O_2 plasma etching; 4) anodization of the patterned aluminum to produce the perfectly-ordered AAO membrane.

processing stages: 1) pattern generation by LIL on a resist layer, 2) pattern transfer into the aluminum substrate, 3) removal of resist layer, and 4) aluminum anodization. The imprint of periodic grooves in the surface guides the pore nucleation process during the first stages of anodization. Under a self-ordering regime, the initial arrangement is kept during the pore enlargement stage, to obtain a perfectly-ordered porous alumina membrane.

The initial state of the surface is essential for successful lithography processing. Electropolished aluminum exhibits a mirror-like surface with nanometric roughness in the order of 10 nm.[38] As a result of the electropolishing hydrodynamics, corrugations in a larger (micrometer) range are also generated. When direct photolithography on the metallic surface is planned, this drawback must be considered. We optimized the electropolishing to maximize the smoothing of the surface and we demonstrated the influence of the residual surface undulations is overcome (see supplementary information).

We used a positive photoresist (PR) layer sensitive to deep UV light to capture the interference pattern generated by LIL. To ensure a homogeneous energy dose along the photoresist profile, a second layer is required and acts as an antireflection coating (ARC). This layer reduces the light reflected power at the PR-ARC interface, which would cause undesired vertical interference phenomena and degradation of the pattern profile. We calculated the reflected power at the PR-ARC interface as a function of the pattern periodicity and the ARC thickness using the optical transmission line formalism method.[37] This facilitates the selection of the bilayer stack layout in a way that the reflected power is minimized. In our system, the optimum ARC thickness is (53 ± 5) nm. Under this configuration, the reflected power is lower than 3% for any periodicity chosen, which is a threshold for successful patterning of the photoresist. Refer to the supplementary information for a more detailed description.

To simplify the LIL process, a Lloyd's interferometer with a two-mirror stage is used.[36] This configuration renders to three-beam interference and directly generates a hexagonal pattern in the PR. **Figure 2**A shows a scheme of the stage and Figure 2B shows the corresponding simulation of the resulting interference pattern. The periodicity (P) of the pattern depends only on the laser wavelength ($\lambda = 266$ nm) and the beam incident angle (θ), given by Equation 1. The symmetry of the interferometer guarantees the periodicity is equal in all three symmetry axes of the pattern. The use of wavelengths in the deep UV region provides the patterns with nanoscaled lattice constants.

$$P = \frac{\lambda}{1.5 \cdot \sin\theta} \quad (1)$$

By rotation of the stage with respect to the incoming laser beam, the periodicity can be tuned from 180 nm up to 1200 nm.

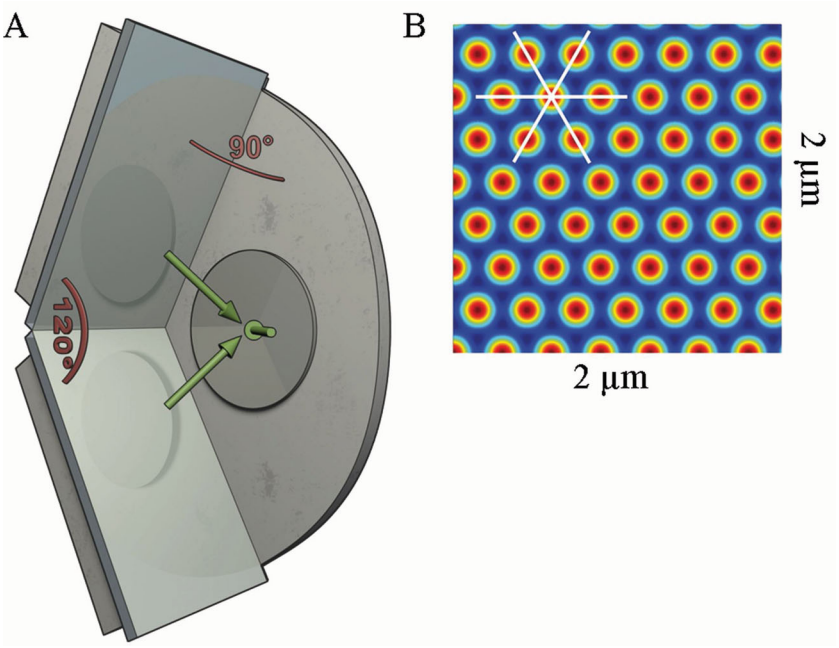

Figure 2. A) 3D scheme of the two-mirror stage used in the LIL setup. The green arrows point out the k-vectors of the incoming and the two reflected plane waves over the aluminum sample. B) Simulation of the periodic hexagonal pattern with periodicity 300 nm generated by the two-mirror stage on the aluminum sample. The three 60°-symmetry axes are pointed out with the white lines. Intensity scale is normalized with respect to the maximum (red) and minimum (blue) values. Note that a positive photoresist would be developed in the red areas, creating holes in the photosensitive layer.

The plot in **Figure 3** combines the experimental periodicity data for the LIL setup and the most common anodization processes. The highlighted area points out the region where the LIL patterns match the anodization windows. Two anodization regimes are suitable: the mild anodization in phosphoric acid bath for the range from 400 nm up to 500 nm,[14,15,17] and the hard anodization in oxalic acid bath for the range from 250 nm and 400 nm. Both processes are self-ordered, guaranteeing the original pattern is not lost. The processes cover a broad range of periodicities embracing from 200 nm up to 500 nm. In this work, we present only our results on the hard anodization due to its upcoming properties (i.e., higher growth rates, broader self-organization window, narrower pores, stronger chemical resistance and superior mechanical stability). Additional information regarding the mild anodization process in phosphoric acid bath can be found in the Supporting Information. We patterned the photoresist layers on the electropolished aluminum substrates with different periodicities in the range from 240 nm to 350 nm (**Figure 4**A–D). The diameter of the holes can be adjusted by tuning the energy dose through the exposure time or the laser power. In agreement with the behavior of a positive photoresist and the interference pattern given in Figure 2B, we observed that for small energy doses, holes that are not completely open at the bottom are formed on the regions of constructive interference. Higher doses resulted in an increase of the diameter of the holes after development and the underneath ARC was fully exposed at the bottom of the holes. An overexposed dose created coalescence of holes and eventually full removal of the photoresist layer. In this work, we found

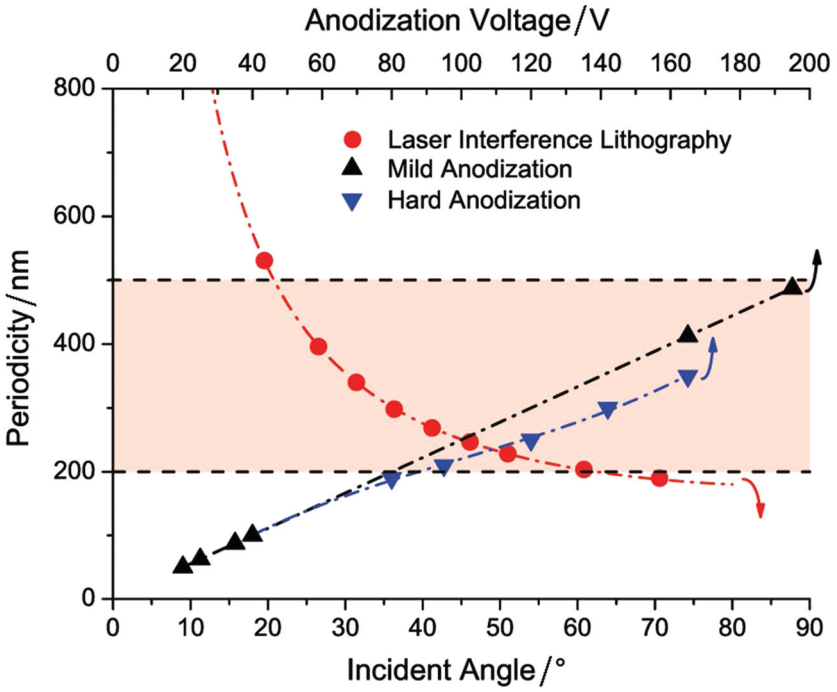

Figure 3. Dependence of the pattern periodicity as a function of the incident angle in the LIL (red line) and the applied anodic voltage for the most standard mild anodization processes (black line) (sulphuric acid at 20–25 V, oxalic acid at 35–40 V and phosphoric acid at 160–195 V) and for the hard anodization regime in oxalic acid bath (blue line). The delimited area points out the region of optimum matching of LIL and anodization in our setup.

the duty cycle—ratio of hole diameter to periodicity—from 40 percent to 60 percent is optimum for successful pore nucleation in the entire area. Due to the broadening of the diameter distribution of the holes caused by the microscaled surface corrugations, working with too high or too low duty cycles results in local coalescence or uncompleted opening of the holes (refer to Figure S2, Supporting Information). This leads to random pore nucleation in the affected areas. An extended discussion is included in the supporting information.

For an optimal anodization process, the aluminum must be exposed to the electrolyte solution from the beginning of the electrochemical process. The ARC is not developed during the PR processing. The resist at the bottom of the holes must be removed to expose the underlying aluminum. Dry-etching using O_2 plasma at low pressures is effective for this purpose. The necessary anisotropic nature of the etching originates from the unidirectional acceleration of the charged species in the plasma perpendicular to the sample surface. The main concern is the thickness ratio between the PR and the ARC. The upper PR layer has to act as a mask for the etching of the underlying layer during the complete etching process. Since both PR and ARC are etched by the O_2 plasma with similar rates, the thickness ratio is set to 3 and a photoresist layer of 180 nm is used. The completely open holes can be seen through the resist bilayer in Figure S3B.

At this fabrication step, the patterned resist stack can be used for the pore nucleation. For a more homogeneous anodization, it is desirable to fully transfer the pattern into the aluminum substrate. This is carried out in two steps. First, exposed aluminum at the bottom of the holes of the resist layer is chemically etched using a diluted alkaline solution, producing nanoconcavities due to the masking effect of the organic layer. Next, the organic layer is completely removed using a long O_2 plasma etching. The resulting surface is characterized by AFM and is shown in Figures 4E,F. It resembles the nanotextured aluminum surfaces obtained by other lithographic approaches.[26,28] The cavities are 15–20 nm deep (see profile in Figure 4G), which are deep enough to induce the guided pore nucleation, as reported by Choi.[39]

In **Figure 5**A,B, we present the top views of the substrates after anodization of the patterned aluminum surfaces for two different periodicities. We successfully applied the strategy allocating the pore nucleation sites through LIL and pattern transfer. Pore nucleation is mainly an effect of the electric field concentration during the first stages of the anodization at the surface nanoconcavities, locally enhancing both, the dissolution and formation of Al oxides.[40,41]

We carried out hard anodization in an oxalic acid bath at high electric fields in the voltage range from 100 up to 190 V, which is above the breakdown voltage of the AAO.[19] These conditions are suited for interpore distances from 200 nm up to 400 nm under a self-organization regime. Compared to the standard mild conditions in oxalic acid at 40 V, it can easily render to uncontrolled anodization and local catastrophic phenomena due to the high electrical current densities and generated heat. Two common strategies to stabilize hard anodization make use of a previously grown porous oxide layer to prevent the flow of high current densities during the first stages of the anodization. We also added alcohol to the aqueous solution to tune the ionic conductivity in the pores.[19,21,42] The preformed oxide layer can be grown using a pre-anodization step carried out under mild conditions, which are stable from the beginning. Phosphoric acid anodization at low voltages can serve this purpose. Even though this range of voltages does not correspond to a self-ordered regime, it has been previously demonstrated that the initial pattern can be maintained for short anodization time for short pore lengths of less than 1 μm.[12,19] In this work, the mild anodization in phosphoric acid bath is carried out at voltages of 100 V up to 140 V, which provides the same range of periodicities given by the LIL and the hard anodization in oxalic acid bath. The triple match of the periodicity and the interpore distances of mild and hard anodization (ID_{Man} and ID_{Han}, respectively) can be accomplished by Equation 1 for LIL, the general relationship in Equation 2 applicable to all self-ordered mild anodization regimes,[15] and Equation 3, which we established for the hard anodization window in oxalic acid bath in the range from 120 V up to 165 V.

$$ID_{MAn} = 2.50 \frac{nm}{V} \cdot V_{MAn} \quad (2)$$

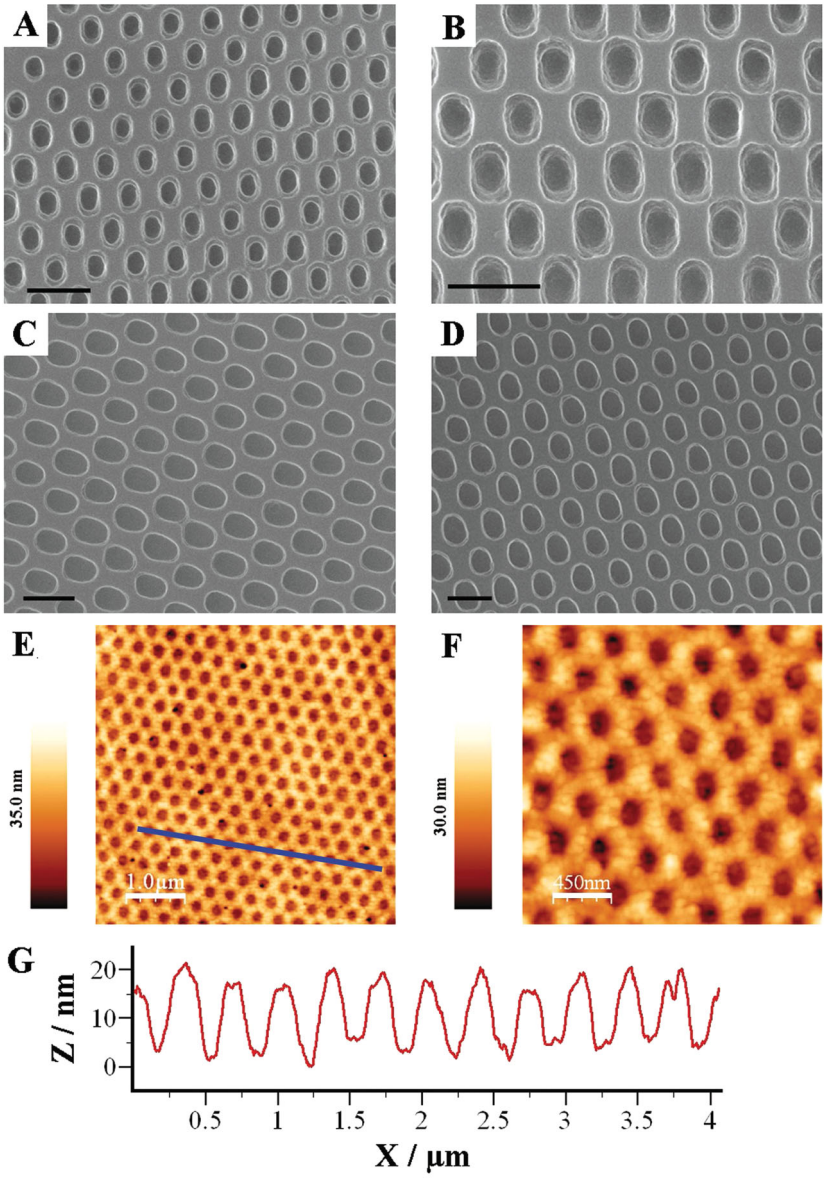

Figure 4. SEM top views of photoresist layers patterned by LIL on electropolished aluminum. The periodicities are A) 240 nm, B) 300 nm, C) 325 nm, and D) 350 nm. Scale bars are 400 nm. E,F) Topographic images at two different scales obtained by AFM in contact mode of the aluminum surface after the wet-chemical etching and complete removal of the resist bilayer stack for a periodicity of 350 nm. G) Height profile taken from the AFM image (E). The average peak-to-peak is 15 nm.

$$ID_{HAn} = 2.22 \frac{nm}{V} \cdot V_{HAn} - 16.2\,nm \quad (3)$$

where V_{MAn} and V_{HAn} are the applied anodic voltages during the mild and the hard anodization, respectively.

Another factor to consider is the thickness of the pre-anodized oxide layer required to prevent the catastrophic phenomena. It plays an important role for stable hard anodization by preventing the initial flow of high ionic currents due to diffusion control in the pores. We experimentally found that a pre-oxide layer with a ratio of thickness to pore diameter equal to or higher than 7 is enough to stabilize the subsequent hard anodization, as long as the cooling system avoids sample overheating since the limiting diffusion currents are temperature dependant. For an interpore distance of 350 nm and pore diameter of 150 nm, at least a 1 µm thick oxide layer is necessary.

The standard mild anodization receipt in phosphoric acid is not suitable to drive the pore nucleation at the nanoconcavities at voltages below 180 V. The anodization must be 'hardened' to induce higher electric fields by increasing the bath temperature and the electrolyte concentration (4% H_3PO_4 at 10 °C instead of 1% at 1 °C), which is translated to an increase in the current density, and therefore, the electric field. The resulting enhancement of the electric field guarantees pore nucleation takes place at the desired surface locations. Since the electric field is the main driving force guiding the self-organization, the initial periodic arrangement is not lost during the growth process of the pre-oxide layer and the oxide growth rate is significantly increased. One must be aware about the fact that there is no time dependence of interpore distance and self-organization in mild anodization, but it is the contrary in the hard anodization. It has already been reported that in hard anodization, interpore distance is influenced by current density and consequently decreases with time.[43,44] This is due to the fact that the electric field and the current density are closely related. While in mild anodization the current is fairly constant and really low, in hard anodization the high diffusion limited ionic currents in the pore result in an exponential decrease of the current as the pore gets longer, which causes a decrease of the interpore distance. For short anodizing times the influence is negligible, but long hard anodization can result in a strong modification of the interpore distance and the original pattern can be partly lost. To avoid this effect the current must be kept constant during the anodization by increasing either the electrolyte concentration or the bath temperature or both.

In Figure 5C,D, the bottom and cross-section views of a perfectly-ordered membrane with a periodicity of 350 nm produced under hard anodization conditions is shown. The 1 µm pre-anodized oxide layer is also visible. The bottom view demonstrates the hexagonal pattern was kept during the anodization process due to the self-ordered regime. The cross-section view magnifications from the pores mouth and the barrier layer (Figure 5E,F) show the high homogeneity of the oxide layer due to the use of a nanotextured aluminum surface as pore nucleation guidance instead of the patterned resist bilayer. The pores show a perfect cylindrical shape with a narrow distribution of diameters around 130 nm. The inset in Figure 5C as well as

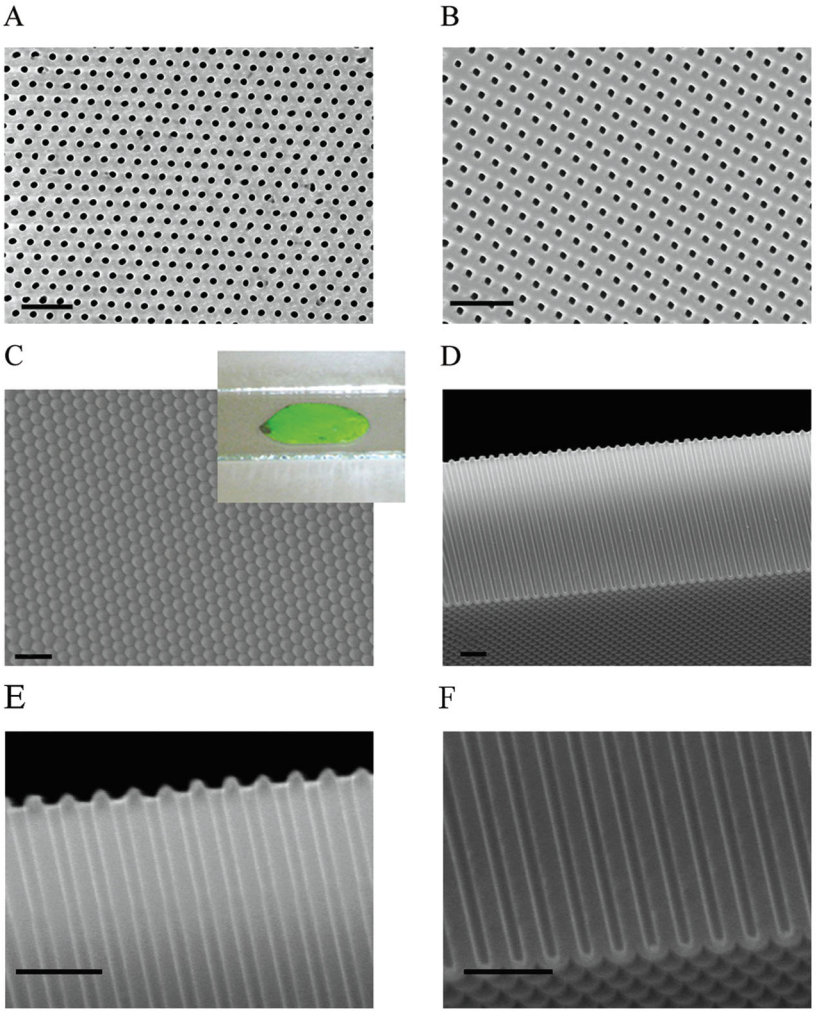

Figure 5. SEM top views of porous AAO membranes with interpore distances A) 300 nm and B) 350 nm. C) SEM bottom view of the barrier layer and D) the membrane cross-section of the membrane with interpore distance 350 nm. Magnified views of E) top and F) bottom sides of the cross-section shown in (D). The inset in (C) shows a free-standing, perfectly-ordered membrane placed in a 2 cm wide microscope slide. All scale bars correspond to 1 µm.

the last photographs in Figure 1 show free-standing membranes after complete removal of remaining aluminum substrate. When illuminated by white light, only a short range of wavelengths are reflected or transmitted: mainly green light for the shown samples with interpore distance 350 and 400 nm, depending on the incident angle and only at certain angles (each 60°, pointing out the hexagonal geometry of the substrate). Thus, the perfectly-ordered AAO membranes behave as photonic crystals and the homogeneity of the long-range order can be qualitatively evaluated from these pictures, as the phenomenon extends over the whole area. More information about the AAOs as photonics crystals has been added to the supporting information.

3. Conclusions

We present a new approach for the fabrication of perfectly-ordered porous alumina membranes with tuned periodicity and thicknesses greater than 1 µm. The effective combination of laser interference lithography patterning on bulk aluminum foils and subsequent anodization provides a versatile template fabrication framework where the periodicity can be adjusted over a wide range of values. We demonstrate the viability of the process for mild anodization in phosphoric acid and hard anodization in oxalic acid, covering a broad range from 250 nm up to 500 nm interpore distances with high accuracy. The process is tolerant enough to be carried out on electropolished aluminum surfaces without prior mechanical polishing steps. In combination with the self-ordered anodization, AAO membranes with aspect ratios higher than 500 are feasible. The process overcomes the limitations of other patterning techniques in regards to size of the areas, range of attainable interpore distances, uniformity, control of geometrical parameters and processing times. These highly-ordered membranes show potential applications for photonic or plasmonic related devices and solar cells. In addition, the high aspect ratios of the pores allow for further implementation to the template-assisted fabrication of 1D nanostructures as free-standing membranes.

4. Experimental Section

Materials: Aluminum (Goodfellow, 99.999%), perchloric acid (ACS grade 70% $HClO_4$), ethanol (ACS grade ≥ 99.5%), GenARC 266 antireflection coating (Brewer Science), UV 2000 positive photoresist (Rohm & Haas), MF CD-26 developer (Rohm & Haas), sodium hydroxide (reagent grade ≥ 98% NaOH), phosphoric acid (ACS grade ≥ 85% H_3PO_4), oxalic acid dihydrate (ACS grade ≥ 99% $H_2C_2O_4{\cdot}2H_2O$) have been used in this work. All chemicals, unless specified, have been purchased from Sigma-Aldrich. All aqueous solutions have been prepared with water obtained from a Millipore RiOs system (15.0 MΩ cm, TOC < 30 ppb).

Patterning of Aluminum by Laser Interference Lithography: Disks cut from pure aluminum foils (1.8 cm or 4 cm in diameter, 0.5 mm thick) were electropolished in $HClO_4$:Ethanol 1:3 (vol.) at 19 V and 10 °C. The antireflection coating and the positive photoresist film, designed for deep UV lithography, were spin-coated on the aluminum surface. Layer thicknesses were controlled by the spin rate and optimized to minimize the reflectivity at the photoresist-antireflection coating interface by the optical transmission line formalism method.[37] The sample was illuminated by a diffracted, highly coherent laser beam (d = 2 mm, λ = 266 nm, VERDI V2 + MBD-266 system from Coherent Inc.) using a custom Lloyd's interferometer with a two mirror configuration.[36] The gaussian beam was focused on a 5 µm pinhole and the resulting diffracted beam at 2 m from the pinhole was large enough to homogeneously illuminate the stage. The irradiated photoresist was developed and the pattern transferred through the antireflection coating using a short O_2 plasma (75 W, 25 sccm, 25 mTorr). The exposed aluminum was chemically etched using NaOH (0.05 M) for 90 s and the remaining resist stack was removed with a long O_2 plasma etching.

Aluminum Anodization in Hard and Mild Regime: The patterned aluminum chips were anodized using different baths and conditions depending on the desired periodicity. H_3PO_4 1–4% wt., 1–10 °C and 160–195 V for 400–490 nm periodicities (self-ordered mild anodization in phosphoric acid bath). $H_2C_2O_4$ 0.15–0.30 M in water:ethanol 3:1 and –5 to 0 °C at 120–165 V for 250–350 nm periodicities (self-ordered hard anodization in oxalic acid bath). The pre-anodized oxide layer was grown in H_3PO_4 4% wt. at 100–140 V and 10 °C for 250–350 nm periodicity (mild anodization in phosphoric acid bath). All anodizations were carried out on one side of the aluminum chip. The other side was in contact with a copper plate used to cool the aluminum and act as the electrical contact. The bath was vigorously stirred and constantly cooled through the copper plate.

Morphological Characterization: We investigated the different structures using a field emission scanning electron microscope (Sigma, from Carl Zeiss AG). For a complete characterization of the membranes, the remaining unoxidized aluminum after the anodization was selectively removed using a $CuCl_2$ 3% wt. in HCl 20% wt. solution. The free-standing membrane was then characterized from the top and the bottom sides. In addition, cross-section views of the membranes were prepared to evaluate the uniformity of the ordered porous structure. AFM images from the patterned aluminum surface were captured in contact mode using a Nanoscope III from Digital Instruments.

Supporting Information

Supporting Information is available from the Wiley Online Library or from the author.

Acknowledgements

We gratefully acknowledge financial support from the German Research Foundation (DFG) via SFB 986 "M^3", project C3, as well as the EU FP7 NMP3-SL-2008–214107-Nanomagma and the Spanish MICIIN: MAT-2010–20798-C05–04. This work was funded by the State of Hamburg through the Cluster of Excellence "Nanotechnology in Medicine" (LEXI NAME). R. Zierold thanks the DFG 616/18–1 for financial support. The authors thank C. Bae for helpful discussions.

Received: September 22, 2013
Revised: October 2, 2013
Published online: November 20, 2013

[1] Y. Wakayama, N. Hiroshiba, R. Hayakawa, T. Chikyow, K. Kobayashi, *Jpn. J. Appl. Phys.* **2012**, *51*, 06FA01.
[2] A. Huczko, *Appl. Phys. A* **2000**, *70*, 365.
[3] V. Grasso, V. Lambertini, P. Ghisellini, F. Valerio, E. Stura, P. Perlo, N. Nicolini, *Nanotechnology* **2006**, *17*, 795.
[4] Y. Lei, S. Yang, M. Wu, G. Wilde, *Chem. Soc. Rev.* **2011**, *40*, 1247.
[5] V. Shklover, L. Braginsky, G. Witz, M. Mishrikey, C. Hafner, *J. Comput. Theor. Nanosci.* **2008**, *5*, 862.
[6] E. Comini, C. Baratto, G. Faglia, M. Ferroni, A. Vomiero, G. Sberveglieri, *Prog. Mater. Sci.* **2009**, *54*, 1.
[7] *Nanotechnology in drug delivery* (Eds: M. M. de Villiers, P. Aramwit, G. S. Kwon), Springer, New York **2009**.
[8] H. Masuda, M. Yamada, F. Matsumoto, S. Yokoyama, S. Mashiko, M. Nakao, K. Nishio, *Adv. Mater.* **2006**, *18*, 213.
[9] D. Chanda, K. Shigeta, T. Truong, E. Lui, A. Mihi, M. Schulmerich, P. V. Braun, R. Bhargava, J. A. Rogers, *Nat. Commun.* **2011**, *2:479*, 1.
[10] D. Choi, Y. Choi, S. Hong, T. Kang, L. P. Lee, *Small* **2010**, *6*, 1741.
[11] Z. Fan, H. Razavi1, J. Do, A. Moriwaki, O. Ergen, Y.-L. Chueh, P. W. Leu, J. C. Ho, T. Takahashi, L. A. Reichertz, S. Neale, K. Yu, M. Wu, J. W. Ager, A. Javey, *Nat. Mater.* **2009**, *8*, 648.
[12] K. Pitzschel, J. M. Montero Moreno, J. Escrig, O. Albrecht, K. Nielsch, J. Bachmann, *ACS Nano* **2009**, *3*, 3463.
[13] K. Pitzschel, J. Bachmann, S. Martens, J. M. Montero Moreno, J. Kimling, J. G. Meier, J. Escrig, K. Nielsch, D. Görlitz, *J. Appl. Phys.* **2011**, *109*, 033907.
[14] K. Noh, K. S. Brammer, T.-Y. Seong, S. Jin, *NANO: Brief Rep. Rev.* **2011**, *6*, 541.
[15] G. D. Sulka, in *Nanostructured Materials in Electrochemistry* (Ed: A. Eftekhari), Wiley-VCH Verlag GmbH & Co. KGaA, Weinheim, Germany **2008**, Ch. 1.
[16] G. E. J. Poinern, N. Ali, D. Fawcett, *Materials* **2011**, *4*, 487.
[17] A. P. Li, F. Müller, A. Birner, K. Nielsch, U. Gösele, *J. Appl. Phys.* **1998**, *84*, 6023.
[18] K. Nielsch, J. Choi, K. Schwirn, R. B. Wehrspohn, U. Gösele, *Nano Lett.* **2002**, *2*, 677.
[19] W. Lee, R. Ji, U. Gösele, K. Nielsch, *Nat. Mater.* **2006**, *5*, 741.
[20] K. Schwirn, W. Lee, R. Hillebrand, M. Steinhart, K. Nielsch, U. Gösele, *ACS Nano* **2008**, *2*, 302.
[21] Y. Li, M. Zheng, L. Ma, W. Shen, *Nanotechnology* **2006**, *17*, 5101.
[22] Y.-C. Ha, D.-Y. Jeong, *J. Korean Phys. Soc.* **2010**, *57*, 1661.
[23] H. Masuda, K. Fukuda, *Science* **1995**, *268*, 1466.
[24] J. Choi, R. B. Wehrspohn, U. Gösele, *Electrochim. Acta* **2005**, *50*, 2591.
[25] A. P. Robinson, G. Burnell, M. Hu, J. L. MacManus-Driscoll, *Appl. Phys. Lett.* **2007**, *91*, 143123.
[26] T. S. Kustandi, W. W. Loh, H. Gao, H. Y. Low, *ACS Nano* **2010**, *4*, 2561.
[27] M. Park, G. Yu, K. Shin, *Bull. Korean Chem. Soc.* **2012**, *33*, 83.
[28] S. Fournier-Bidoz, V. Kitaev, D. Routkevitch, I. Manners, G. A. Ozin, *Adv. Mater.* **2004**, *16*, 2193.
[29] W. Lee, R. Ji, C. A. Ross, U. Gösele, K. Nielsch, *Small* **2006**, *2*, 978.
[30] Y. He, X. Li, L. Que, *J. Nanosci. Nanotechnol.* **2012**, *12*, 7915.
[31] Z. Sun, H. K. Kim, *Appl. Phys. Lett.* **2002**, *81*, 3458.
[32] A. Rodriguez, M. Echeverría, M. Ellman, N. Perez, Y. K. Verevkin, C. S. Peng, T. Berthou, Z. Wang, I. Ayerdi, J. Savall, S. M. Olaizola, *Microelectron. Eng.* **2009**, *86*, 937.
[33] J.-M. Park, Z. Gan, W. Y. Leung, R. Liu, Z. Ye, K. Constant, J. Shinar, R. Shinar, K.-M. Ho, *Opt. Express* **2011**, *19*, A786.
[34] J. Henzie, M. H. Lee, T. W. Odom, *Nat. Nanotechnol.* **2007**, *2*, 549.
[35] D. J. Lipomi, R. V. Martinez, L. Cademartiri, G. M. Whitesides, in *Polymer Science: A Comprehensive Reference* (Eds: K. Matyjaszewski, M. Möller) Elsevier B.V., Oxford, UK **2012**, Ch. 7.11.
[36] J. de Boor, N. Geyer, U. Gösele, V. Schmidt, *Opt. Lett.* **2009**, *34*, 1783.
[37] J. A. Davies, B. Domeij, J. P. S. Pringle, F. Brown, *J. Electrochem. Soc.* **1965**, *112*, 675.
[38] J. P. W. O'Sullivan, G. C. Wood, *Proc. R. Soc. Lond. A* **1970**, *317*, 511.
[39] J. Choi, PhD thesis, Martin-Luther-Universität, Halle, Wittenberg **2004**.
[40] J. M. Montero-Moreno, M. Sarret, C. Müller, *Surf. Coat. Technol.* **2007**, *201*, 6352.
[41] S. Ramo, J. R. Whinnery, T. van Duzer, in *Fields and Waves in Communication Electronics*, Wiley, New York **1994**.
[42] Y. Li, Z. Y. Ling, J. Wang, S. Chen, X. Hu, X. He, *Chinese Sci. Bull.* **2008**, *53*, 1608.
[43] K. Schwirn, W. Lee, R. Hillebrand, M. Steinhart, K. Nielsch, U. Gösele, *ACS Nano* **2008**, *2*, 302.
[44] Y. Li, M. Zheng, L. Ma, W. Shen, *Nanotechnology* **2006**, *17*, 5101.